Experimental Investigation of the Flowfield Behind Grid Models

Hiroshi Higuchi*
University of Minnesota, Minneapolis, Minnesota

The flowfield past flat and curved grid models simulating segments of a ribbon parachute was investigated experimentally. Flow visualizations and surface pressure measurements were conducted to study the effect of the spacing ratio and the Reynolds number. Irregular and unstable flow patterns existed behind the flat grid model at high solidity configurations. The results of the curved grid model indicated a stabilizing effect of the grid curvature. In addition, a flow visualization study on the flowfield behind a slotted disk model was conducted. The cross-sectional view of the wake showed strong similarities to the wake behind the two-dimensional grid models; its wake pattern is discussed.

Introduction

THE flowfield immediately downstream of a ribbon parachute is more complex than that of a solid parachute because of irregular merging of high-speed jets through multiple narrow gaps. The recirculation zone, transverse swirling eddies, and jets through canopy slots coexist. Though detailed knowledge of the wake structure is essential to understand and avoid such problems as the wake recontact problem,[1] analysis of the entire wake region at once appears so far to be inaccessible. Thus, various elements of the flowfield are presently being studied as building blocks toward a full understanding of the flow behind the parachute canopy.

In general, high solidity screens are known to produce a high level of turbulence and thus have been avoided for wind-tunnel use,[2] but some flow configurations inherently involve the flow pattern past multiple narrow gaps, such as flow past ribbon parachutes. Merging and biasing of two-dimensional multiple jets were first reported by Bohl[3] and Corrsin[4] and more recently by Hayashi et al.[5] In addition, nonuniform pressure distributions have been measured by Roberts[6] on a slotted disk simulating a ribbon parachute. The numerical simulations for two-dimensional and axisymmetric flow past some elements of parachute have been attempted (see, for example, summary of vortex methods in Ref. 7), but, so far, the physics of the wake flowfield has not yet been fully understood nor has it been incorporated in simulations currently available.

Therefore, the present experimental investigation was initiated to study parametrically the flowfield behind the various simplified configurations in the order of increasing complexity to shed some light on the complex wake flow behind the ribbon parachute. In this study, the elements of the ribbon parachute were first simulated by a row of many closely spaced flat plates. Complex irregular flow patterns existed even behind the simple flat grid models, and they were found highly transient and subject to the external disturbances and hysteresis effects.[8,9] The flow past the flat grid models was found to be very sensitive to the spacing ratio. The effect of curvature was then studied with a curved row of the flat plate elements. While the experiment on the fundamental flowfield of these grid models at various configurations is being continued, a parallel work to probe the three-dimensional flow behind more representative axisymmetric models has been initiated. The results of the flow visualization behind a slotted disk are presented in this paper and compared with the two-dimensional counterpart. The general feature of the flow has been found to be common to both studies.

The present study was carried out in incompressible flows at moderate Reynolds numbers, but it is to be noted that vortex interaction phenomena appear to be less sensitive to the Reynolds number, and that aircraft flight data have compared well with water dye flow visualizations in the past.[10] Naturally, the present rigid elements on the two-dimensional and axisymmetric grid models cannot fully simulate the actual ribbon parachute elements, which are porous and flexible. Though there are many effects that are to be incorporated for a practical design purpose, it is hoped that the present results will point out some fundamental aspect toward that goal.

Experimental Setup and Techniques

Facilities

The experiment with the two-dimensional grid models was conducted in a low-speed, open-return wind tunnel. The test section of the open-return tunnel is 1.83 m long with a 30.5×43.2 cm cross section. Maximum speed of about 70 m/s can be obtained within an empty test section, but, when the high solidity grid model was in place, the maximum velocity was substantially reduced. Freestream turbulence was between 0.3 and 0.6%, and mean flow uniformity was better than 1%.

A low-speed, closed-return wind tunnel was also used for flow visualization studies with axisymmetric models. The closed test section measures 1.37×0.97 m and freestream velocity up to 49 m/s can be obtained. The turbulence level in this tunnel was about 0.8% and flow nonuniformity up to $\pm 5\%$ existed away from the center region of the test section, but they were still adequate for the flow visualization study.

Test Models

Two-Dimensional Grid Models

Two types of grid models were tested at various incoming velocities and gap ratios; these were a normal row of flat plates and a curved row of flat plates. These different models are schematically shown in Fig. 1. Each flat plate representing the grid element was made of aluminum and measured 12.7 mm high, 3.2 mm thick, and 305 mm long. Leeward side corners were leveled off by 20 deg. Individual plates were placed

Presented as Paper 86-2460 at the AIAA 9th Aerodynamic Decelerator and Balloon Technology Conference, Albuquerque, NM, Oct. 7-9, 1986; received Jan. 9, 1987; revision received June 15, 1988.

*Assistant Professor, Department of Aerospace Engineering and Mechanics. Member AIAA.

either normal or at varying pitch angles to the incoming flow, depending on the model type, and spanned the entire cross section. The height of the individual plate is hereafter denoted by h. Individual plates were instrumented with pressure taps on the front and rear sides. Pressure distribution on the model was measured simultaneously on the manometer board as well as with electronic pressure transducers.

In order to provide a two-dimensional flowfield, thin side plates were placed 25.4 mm from the side walls of the tunnel. The tunnel wall boundary layers were thin and boundary-layer effects at the top and bottom walls were found to be negligible.

Normal Row of Flat Plates (Flat Grid Models)

This model, as shown in Fig. 1, consists of numbers of flat plate elements placed parallel to each other on a plane separated by various heights of spacers to achieve given spacings s. The model assembly extended over the entire height of the test section. End conditions were such that the model would simulate an infinite row of plates, and each model contained sufficient number of elements to avoid the end effects. The results on the flat grid models with smaller spacing ratios ($s/h \leq 1$) will be presented herein, though models with other spacing ratios were also tested. Porosity of the models in this case varied from 20 to 50%.

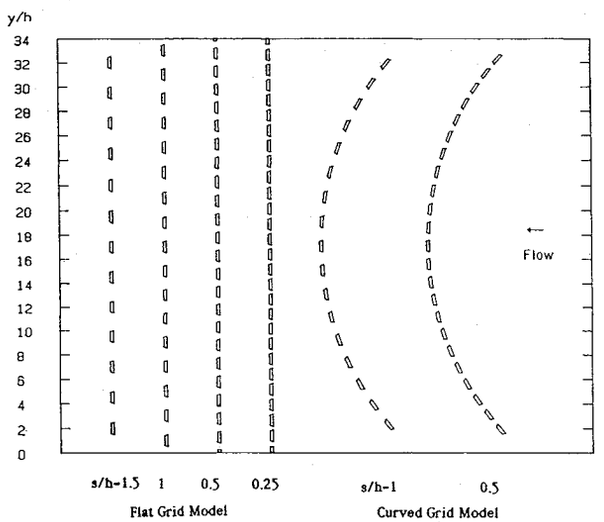

Fig. 1 Grid model configurations.

Curved Grid Models

The individual plates were arranged in a circular arc pattern as shown in Fig. 1. (Figure 6a shows a photograph of the model in the test section.) The radius of the model curvature was 291 mm, so that one plate height forms a 5 deg center angle with respect to the center of curvature. Two spacing ratios, $s/h = 1.0$ and 0.5, were tested with 17 or 23 elements. Equal space was left between the model and the tunnel top and bottom walls. Porosity of the model was 54.4% for the $s/h = 1.0$ case and 38.5% for the $s/h = 0.5$ case. More detailed dimensions for these curved models and flat models are given in Ref. 9.

Slotted Disk Models

As an example of axisymmetric grid models, slotted disk models were tested. One model, machined out of 1 mm thick steel, measured 318 mm in diameter. Each of eight annular grid elements was 12.7 mm wide, which was the same as in the two-dimensional models, and the spacing ratio was 0.5. A center opening measured 25.4 mm in diameter. Four 3 mm wide radial cross elements were placed 90 deg apart between the grids for a support, but their effect on the wake was not perceptible and deemed negligible. The model was supported at the center of the test section of the low-speed recirculating wind tunnel by thin piano wires.

Flow Visualizations

Most of the flow visualizations in air past the two-dimensional grid models were carried out by oil flow visualization technique at the same Reynolds numbers as in the pressure measurements, which ranged from 4800 to 23,000 based on the individual element height. After two-dimensionality of the flow was verified, a 2.5 mm thick splitter plate was mounted vertically immediately downstream of the model at the midspan position, and a mixture of titanium dioxide and mineral oil was applied on the plate. In some selected cases, tufts were used to check the spanwise flow variations and the size of the large recirculation bubbles downstream of the model.

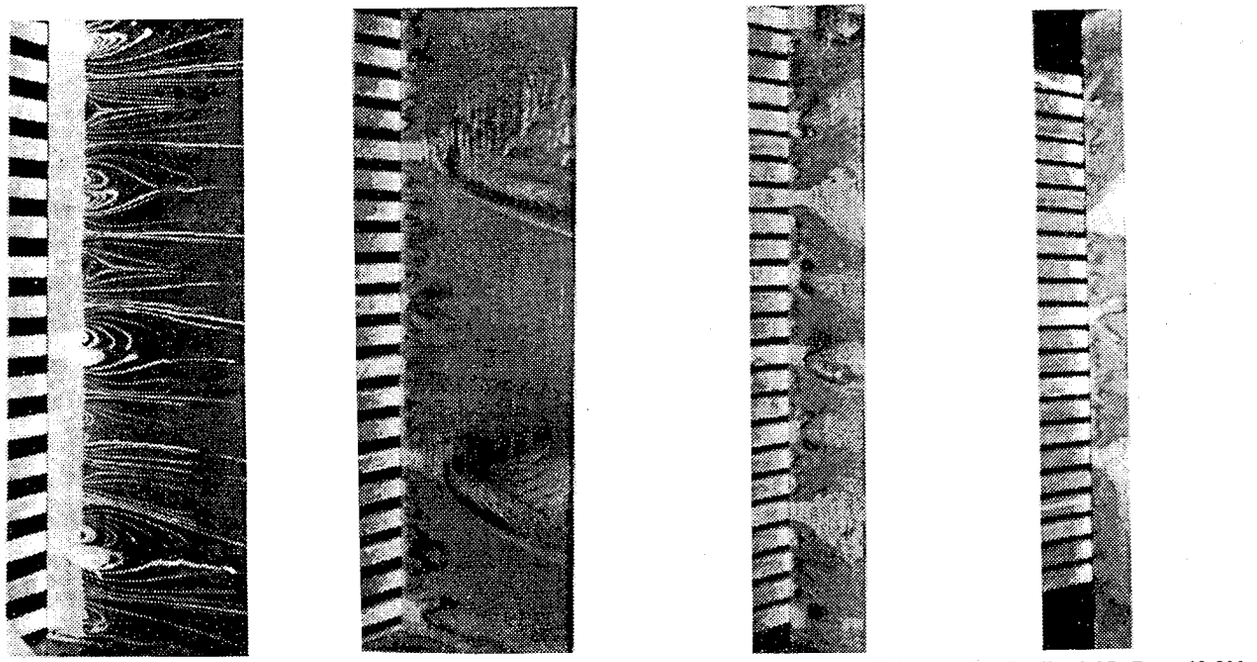

a) $s/h = 1$, $Re_h = 23{,}500$ b) $s/h = 11.5$, $Re_h = 11{,}100$ c) $s/h = 0.25$, $Re_h = 7300$ d) $s/h = 0.25$, $Re_h = 13{,}300$

Fig. 2 Oil flow visualizations behind flat grid models (top and bottom vented).

Flow visualization past the axisymmetric model was conducted by injecting fog upstream of the model and illuminating with a sheet of laser light. A Rosco fog generator was used. Cross-sectional illumination was provided with an argon-ion laser beam past through a set of cylindrical lenses. Freestream velocity was varied between 2 and 20 m/s. This higher speed gives the Reynolds number of 4×10^5 based on the model diameter and 1.6×10^4 based on the individual grid width.

Results

Flat Grid Models

For all the flat grid models except for the case in which flow was vented at the top and bottom walls, the flowfield and the windward pressure distribution of the model were uniform (see Fig. 3 for $s/h=1$, for example, and note $C_p\approx1$ at the center of each element), and symmetric and similar pressure distribution was found on each element. On the other hand, as the oil flow visualizations in Fig. 2 for $s/h=1$, 0.5, and 0.25 show, the leeward flowfield exhibited irregular sizes of recirculation zones and was strongly affected by the spacing ratios. Figure 3 shows the windward and leeward pressure distributions for $s/h=1$ and, while the same windward pressure distributions existed on the individual elements of the model as noted earlier, the leeward pressure distributions at these small spacing ratios became highly irregular. (Since the leeward pressure was measured to be almost constant over each element, only the data at the center are shown.) Three levels of pressure magnitude are observed, and these leeward pressure distributions were consistent with the flow visualizations showing mean streamline curvatures of recirculation zones of mainly three different sizes behind individual plate. Moreover, some flow patterns were unstable and transformed into another pattern naturally or by external disturbances. The pressure pattern in Fig. 3 is one of the most frequently observed, and Fig. 4 indicates an example of a hysteresis effect at $s/h=1$, when the incoming freestream velocity was continuously varied and brought back to the original value. At yet smaller spacing ratios, the flow entrainment required by neighboring jets produced large recirculation zones, each starting at a particular element with certain intervals. Representative leeward pressure distributions are shown in Figs. 5a and 5b), where the pressure minima correspond to the large recirculation zones. A variety of other pressure patterns was observed, with minor differences in positions and arrangements of the individual recirculation zones. Detailed pressure distributions and their sensitivity to the external disturbances are given in Ref. 9. The hot wire velocity profile survey confirmed the size and location of the recirculation zones.

At these small spacing ratios, the blockage effect of the model was extremely high as indicated on the large recirculation zones (Figs. 2a and 2c) and on the high mean pressure drop (Figs. 5a and 5b). The effect of the reduced blockage was studied with vented flow on both sides of the model. Four plates were removed at the top and bottom ends of the model, increasing the overall porosity from 20 to 35%. The windward pressure showed decreasing pressure distribution toward the edges corresponding to diverging streamlines ahead of the model.[9] The leeward side pressure distribution is shown in Fig. 5c. A few other profiles were also observed with small shift in the location of the center recirculation zone, but the mean base pressure remained almost identical among all of them. Besides reduced mean pressure drop and medium-sized recirculation zones located almost invariably behind the outermost elements, the leeward pressure profile behind 22 plate elements remained approximately the same as the complete model without vented flow (see Fig. 5c). The flow visualizations with and without the vented flow were also similar, as shown in Figs. 2c and 2d. Therefore, the present results are expected to be also a fairly good representattion of the flowfield immediately behind a finite size model, provided the model contains a large number of elements.

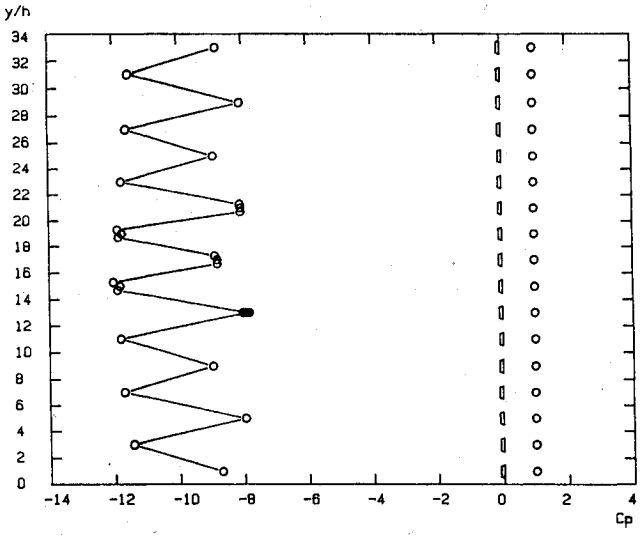

Fig. 3 Windward and leeward pressure distributions at $s/h=1.0$ and $Re_h=22{,}900$.

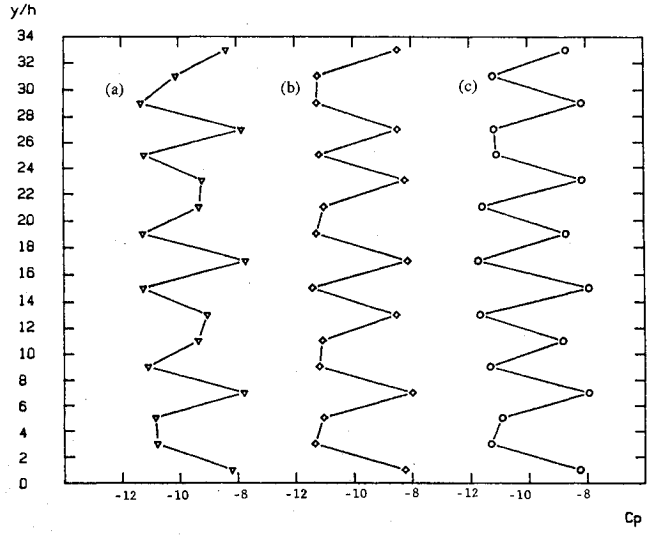

Fig. 4 Hysteresis effect at $s/h=1.0$. [Profile (a) $Re_h=18{,}900$ changed to (b) Re_h22,900 by increasing the speed. Profile (b) changed to (c) Re_h18,900 by decreasing the speed.]

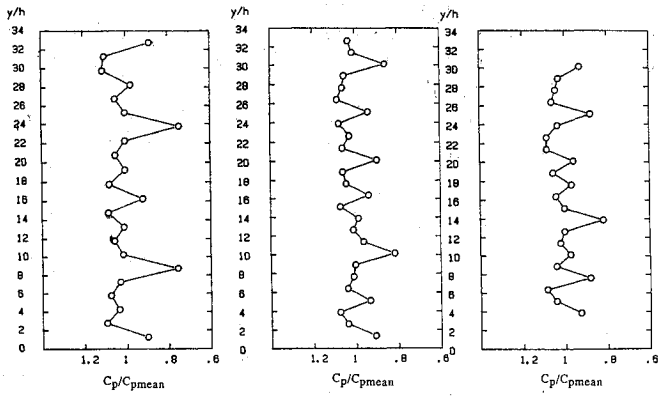

Fig. 5 Leeward pressure distributions at $s/h=0.5$ and 0.25.

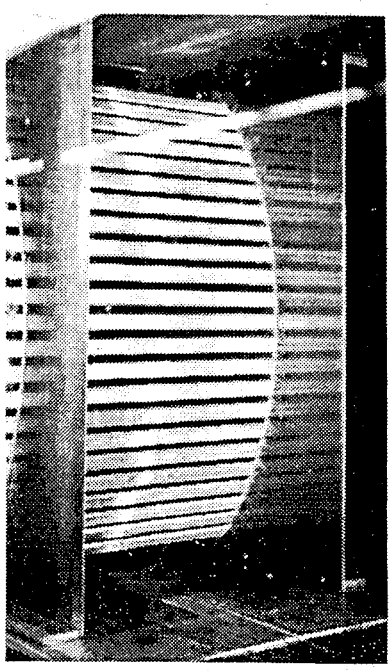

a) Curved grid model in the test section

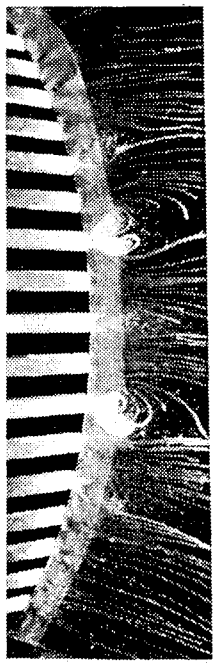

b) $s/h = 1$, $Re_h = 25{,}400$

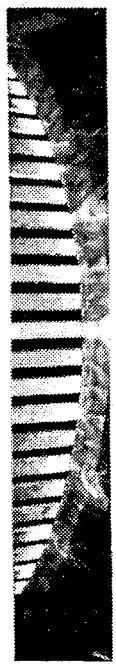

c) $s/h = 0.5$, $Re_h = 16{,}900$

Fig. 6 Oil flow visualizations behind curved grid models.

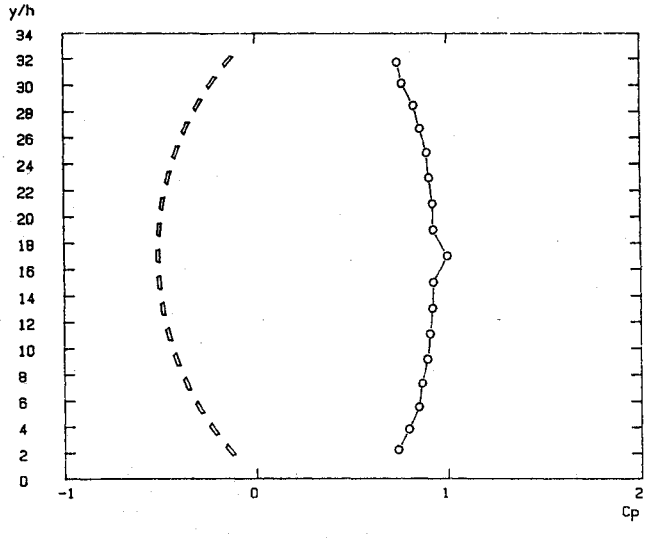

Fig. 7 Windward pressure distribution on curved model of $s/h = 1$.

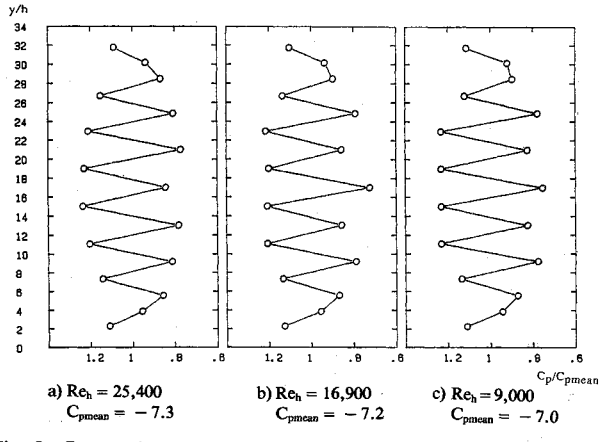

Fig. 8 Leeward pressure distribution on curved model of $s/h = 1$.

Curved Grid Models

The curved model with a radius of curvature of 29.1 cm was tested at two spacing ratios, $s/h = 1.0$ and 0.5. Oil flow visualization was conducted by installing a contoured splitter plate at midspan, and the results are shown in Figs. 6a and 6c together with the grid model in the test section. At $s/h = 1$, the flow pattern was symmetrical about the center plate behind which a medium-sized recirculation zone was found. Two large recirculating regions were located behind the plates second from the center on each side (Fig. 6b). At $s/h = 0.5$ (Fig. 6c), large recirculating zone was always located behind the center plate, while the size of the large recirculating zones was considerably reduced from that behind the flat grid model of the same spacing ratio.

The pressure profiles for these cases were constantly monitored with the manometer board. The results for two spacing ratios are presented separately below. In both cases, the global flow pattern behind the curved model was repeatable, unlike that behind the flat grid models. Even though the flow pattern was found to be still irregular, no unstable variation of the flowfield or hysterisis effect was observed.

Spacing Ratio $s/h = 1$

The pressure distribution on the windward size measured at the center of the individual plates is shown in Fig. 7 together with the schematics of the model. Individual pressure distribution on each element was asymmetric except for the center element, as expected. It can be seen in the figure that the pressure coefficient at the center of each element increases toward the center of the model and approaches the stagnation pressure.

The pressures on the leeward side of the model are shown in Figs. 8a and 8c for Reynolds numbers of 25.4×10^4, 16.9×10^4 and 9×10^3, respectively. (Pressure at the center of each element represents the leeward pressure, which was almost constant over the respective element.) The only difference among these profiles is the magnitude of pressure at the center plate relative to the two neighboring ones. Furthermore, at

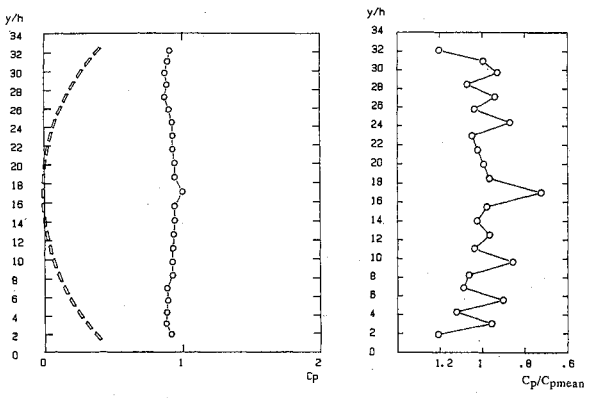

a) Windward b) Leeward, $C_{pmean} = -15.2$

Fig. 9 Windward and leeward pressure distributions on curved model of $s/h = 0.5$ at $Re_h = 16{,}800$.

$Re = 24.3 \times 10^4$, both types of profiles near the center of the model alternately occurred with an approximately 20–30 s period. In all cases, only symmetric types of profile were observed independent of Reynolds number. These profiles were also stable, even with external disturbances. The alternating pressure patterns observed here, except near the edges, were similar to those for the flat grid model at a larger spacing ratio,[9] $s/h = 1.5$.

Spacing Ratio $s/h = 0.5$

As shown in Fig. 9a, windward pressure distribution was uniformly closer to the stagnation pressure compared to the higher porosity case.

The pressure profile most frequently observed on the back side of the model is shown in Fig. 9b. Essentially the same profile was observed at a different Reynolds number of 9.1×10^3. Very infrequently, some other pressure profiles occurred, and all of them changed to that of Fig. 9b after a short time.

Slotted Disk Models

Flow visualizations on axisymmetric models are being conducted with a variety of techniques. A laser sheet was employed to illuminate the wake cross section, and an example of typical flowfield behind the slotted disk model is shown in Fig. 10 taken at a moderatly low Reynolds number. Immediately downstream of individual annular elements, the photograph shows interactions of jets through individual slots, forming irregular distribution of the recirculating zones. These jets further merge in the near wake. The flow closer to the centerline axis of the disk converges toward the center of the wake, while the flow outside this recirculating zone is deflected toward the outer edge. In between these deflected jets, two large recirculating zones, one on each side of the radii, are observed as dark areas in the near wake. This cross-sectional view of irregular recirculating zones behind individual elements is very similar to the flow behind the two-dimensional flat grid model of comparable spacing ratio presented earlier. Further downstream, these merged jets appear to lose momentum and global reverse flow region starts approximately 1.5 diameters downstream of the disk. The leading edge of this downstream reverse flow region could be clearly identified on the video, and the character of this detached recirculation zone was distinguishable from the wake of a solid disk. No distinct vortex shedding was observed. The reverse flow region is terminated further downstream and, approximately 3 diameters downstream of the model, the flow was highly unsteady but was mainly in the downstream direction.

Fig. 10 Flow visualization behind a slotted disk model ($Re = 45{,}000$ based on the model diameter).

Discussion

Effects of Spacing Ratio on the Flat Grid Models

A uniform wake pattern existed at the large spacing ratio of $s/h = 2$. With the decreased opening areas at smaller spacing ratios, however, each jet no longer retains sufficient mass flow required to supply the entrainment in the wake and begins to interfere with adjacent wakes. These wake interaction phenomena observed behind the flat grid models at various spacing ratios are summarized in the following.

Regular alternations between large and small wakes occurred at a spacing ratio of 1.5. When the spacing ratio was further reduced to $s/h = 1.0$, irregular and unstable flow patterns were observed. In some cases, the near-wake pattern flip-flopped, causing oscillating phenomena with a period ranging from a few seconds to a few minutes.

At $s/h = 0.5$ the alternating pressure pattern was no longer present. Large recirculating zones extended far downstream and their stationary positions made the flow pattern generally stable, though some transient flow pattern was observed. In the case of $s/h = 0.25$, the smallest spacing ratio tested, the large and medium recirculation bubbles were at closer intervals than at $s/h = 0.5$. For these small spacing ratios, where the individual openings are smaller than the plate height, the flow downstream of the plates could be regarded as multiple jets rather than an array of wakes. In the smaller $s/h = 0.25$ case, width of jets through gaps decreased, but the distance between jets increased at this spacing ratio. This appeared to reduce the interactions between jets, allowing the formation of alternating patterns. Unlike at other larger spacing ratios, strong spanwise variations in bubble size and suction pressure were observed on the leeward side of the plate with a small recirculation bubble.

Hayashi et al.[5] carried out the flow measurements with a finite-size model consisting of two to five plates placed in the open section of the tunnel. A uniform flow pattern took place for $s/h \geq 2$ when the number of plates was less than five. As the spacing ratio was reduced, the gap flow was biased upward or downward in a stable manner. Since their model size was small compared to the cross section of the tunnel, it could be regarded as a single flat plate with slits where the incoming stream is allowed to flow around the model, while the present

model covers the entire cross section of the upstream flow. In spite of this basic difference in the boundary conditions, a general agreement was achieved between the two experiments including the minimum spacing ratio for the uniform wake patterns. In Corrsin's experiment[4] on the multiple jets issuing from two dimensional slots, the adjacent jets grouped together immediately downstream of the slots and the adjacent groups of jets joined again at a short distance downstream. Corrsin argued that the static pressure between jets was reduced by jet entrainments, and this resulted in jet mergings, which is backed by the present measurements.

Effects of Model Curvature

Effect of curvature was studied on the models extending over the test section. The curvature on the model directed the incoming flow toward the center of the model and this, in turn, strongly influenced the flow downstream of the model. At $s/h=1.0$, the flow always showed a regular alternating and very stable pattern, though for the normal flat plates at the same spacing ratio, the flow pattern was irregular and unstable. Also, for the curved plates at $s/h=0.5$, considerable differences from the normal plates at the same spacing ratio were noted; only one large recirculation zone was found fixed at the center for the curved plates, and the irregular sizes of small recirculation zones behind the flat plates were replaced by a "semiregular" alternating pattern behind the curved plates. It appears that the curvature of the model made the flow downstream stable by forcing the incoming flow toward the cener. Jets through individual slots were measured to be almost equal in their strengths past the flat grid model,[9] while they varied in their strengths and directions past the curved models. A minute disturbance could trigger the bistable condition of the flat grid model (in principle, any irregular flow pattern could be shifted up or down on an "infinite" row of plates on flat grid models), but such triggering was no longer effective to change the flow pattern in the presence of the definite mean flow variation. In addition, the interference among the vortex streets, regarded as a major cause of the instability phenomena similar to that behind the present flat grid model, have been likely reduced behind the curved grid model due to the staggered vortex shedding arrangement.

It is to be noted that, due to the wall proximity, the present model in effect simulated a multiple row of curved arcs; therefore, one should be cautious in comparing the present results with the flowfield of a wake behind a curved model in an unrestricted freestream that allows larger transverse motion of the wake.

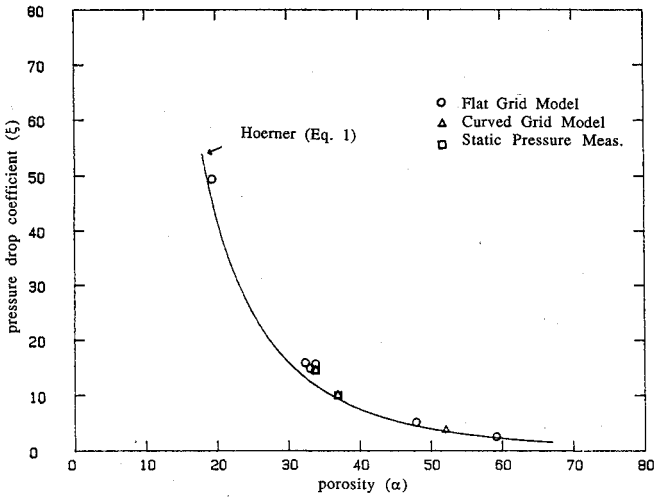

Fig. 11 Pressure drop coefficient across two-dimensional models.

Model Porosity and Induced Pressure Drop

The axial static pressure distributions upstream and downstream of the two representative two-dimensional grid models were measured along the tunnel wall. The static pressure was nearly constant upsteam of the model and dropped to a minimum immediately downstream of the model. At far downstream, the static pressure was constant again after a slight recovery. The values for the pressure drop coefficient were found to be almost independent of the Reynolds number.

Since the present grid model with a group of plates placed in the tunnel test section can be regarded as a special type of screen, the pressure drops due to the grid model are expected to follow a general law of the screens. While there have been several formulas for pressure drop coefficient across the porous screen, a simple formula by Hoerner[11] for pressure drop coefficient $\xi=(\Delta p/q^2)$ as a function of solidity σ of the sharp-edged screen is cited as follows:

$$\xi=(0.5+\sigma)^2/(1-\sigma)^2 \tag{1}$$

The pressure drop coefficients directly measured for the flat and curved grid models at $s/h=0.5$ are shown in Fig. 11 and, compared with Eq. (1), plotted in terms of the overall model porosity $\alpha(\alpha=1-\sigma)$. (The present model porosity data take into account additional blockages such as side plates, but these are less than 4% of the model solidity. For curved models, the projected porosity is used.) In addition, the pressure drop coefficients for the present grid models at other spacing ratios can be obtained from the pressure measurements on windward and leeward sides of the models. The average leeward side pressure distribution and the average pressure on the windward face of each grid element were used.

The pressure drop coefficients obtained are compared with a curve of Eq. (1). The good agreement with Eq. (1) shows that the overall pressure drop coefficient of a model can be determined by only the model porosity, regardless of the particular pressure distribution or the model curvature, and is independent of irregular distributions of the recirculating region behind independent elements. It must be noted, however, that the present results involve a large number of plate elements (approximately 17–27 elements) extending over the test section, and that the drag coefficients of the model, consisting of small number of elements placed in an unconfined stream, have been found to depend on the number of elements and the particular flow patterns at a given Reynolds number in both two-dimensional[5] and axisymmetric[6] cases.

Flow Past Slotted Disk Models

The near-wake region past the disk was very similar in the cross-sectional plane to that observed in the two-dimensional grid models, and it showed the deflections of jets through the slits forming various sizes of recirculation zone behind each element. Behind the flat grid models at high solidity, large separated zones started from certain elements, increasing in size downstream; this was also observed behind the slotted disk. Though information on the downstream flowfield was not provided, irregular leeward pressure distributions reported by Roberts[6] on the slotted disk recirculating zones were consistent with the present observation. In particular, the stronger negative base pressure near the edge of Roberts' 18-slot case suggests the outer jets deflected toward the edge, which was presently observed. On the other hand, the center element of his model was solid and was larger in radius than the widths of the annular elements, and direct comparison of the flow near the center with the present model was not possible. When the center vent was closed on the present model, a large annular recirculation zone was still present, but the merged jets near the center were more unsteady and whirled about the axis. Whether a large recirculation zone existed or not could not be detemined from the pressure distributions.

Using a pulsed hot wire along the wake centerline of two-dimensional porous plates, Castro[12] has measured two stagnation points indicating a detached reversed flow bubble. In the present flow visualization behind the slotted disk, the global reverse flow region was observed to start and end at some downstream positions of the model, similar to that schematically depicted for two-dimensional porous plate by Castro. Porosity of the disk was not varied suffiently at present to determine the variation of the position of the reverse flow region as a function of porosity.

In addition, as indicated by Oswald and Kibens[13] for the wake behind a solid disk, a fully three-dimensional structure is expected behind a slotted disk further downstream, and an instantaneous flow pattern appears to show axisymmetric ring vortices starting to tilt downstream. This, however, awaits further study since an emphasis was placed presently on the cross-sectional structure of the near-wake regions.

Our study is being continued to determine better the structure of the parachute wake, but clearly the flow past the slotted models appears to be far more complex than solid models due to the jets through the orifice, even when the model is nondeformable and is subject to the steady freestream velocity. It is hoped that the results of the present study may give some insights to practical design problems with certain precautions as to the scale effect.

Conclusions

Flowfield past two-dimensional and axisymmetric grid models was investigated experimentally. In two-dimensional configurations, both flat grid models and curved grid models were studied.

At high-solidity configurations ($s/h \approx 1$), multiple flow patterns were observed even under the same conditions. When the spacing became yet smaller ($s/h = 0.5$ and 0.25), the flowfield was dominated by the presence of the large separated flow regions.

Curvature of the grid model appeared to stabilize the flow pattern, though the pattern is still irregular.

The flowfield behind a slotted disk bore a cross-sectional near-wake pattern similar to that observed downstream of the two-dimensional grid models with discrete mergings of jets but further convoluted due to the three-dimensional wake structures. Further study is still needed for the understanding of the flow behind both basic and practical geometries.

Acknowledgment

The present study was supported by Sandia National Laboratories with Drs. J. Purvis and C. Peterson as technical monitors. Their encouragement on the project is greatly appreciated.

References

[1]Spahr, H. R. and Wolf, D. F., "Theoretial Analysis of Wake-Induced Parachute Collapse," AIAA Paper 81-1922, Oct. 1981.

[2]Laws, E. M. and Livesey, J. L., "Flow Through Screens," *Annual Review of Fluid Mechanics,* Vol. 10, 1976, pp. 247–266.

[3]Bohl, E. V., "Das Verhalten Paralleler Lufstrahlen," Ingenieur-Archiv, XI, Band 1940, pp. 295–314.

[4]Corrsin, S., "Investigation of the Behavior of Parallel Two-Dimensional Air Jets," NACA War Time Report W-90, Nov. 1944.

[5]Hayashi, M., Sakurai, A., and Ohta, Y., "Wake Interference of a Row of Normal Flat Plates Arranged Side by Side in a Uniform Flow," *Journal of Fluid Mechanics,* Vol. 164, March 1986, pp. 1–25.

[6]Roberts, B. W., "Drag and Pressure Distribution on a Family of Porous, Slotted Disks," *Journal of Aircraft,* Vol. 17, June 1980, pp. 393–401.

[7]Strickland, J. H., "On the Utilization of Vortex Methods for Parachute Aerodynamic Predictions," AIAA Paper 86-2455, Oct. 1986.

[8]Higuchi, H. and Kim, H. J., "Pressure Distribution on Leeward and Windward Sides of a Row of Closely Spaced Normal Flat Plates," AIAA Paper 86-0352, Jan. 1986.

[9]Kim, H. J. and Higuchi, H., "Flow Visualization and Mean Pressure and Velocity Measurements Behind the Grid Models," Dept. of Aerospace Engineering and Mechanics, Univ. of Minnesota, TR AEM-H86-1, April 1986.

[10]Werlé, H., "Visualisation des Ecoulements Tourbillonnaires Tridimensionneles, AGARD-FDP on Aerodynamics of Vortical Type Flows in Three Dimensions, the Netherlands, April 1983.

[11]Hoerner, S. F., "Fluid Dynamic Drag," New Jersey, 1965. (Contact author for more information.)

[12]Castro, I. P., "Wake Characteristics of Two-Dimensional Perforated Plates Normal to an Airstream," *Journal of Fluid Mechanics,* Vol. 46, Part 3, April 1971, pp. 599–60910

[13]Oswald, L. J. and Kibens, V., "Turbulent Flow in the Wake of a Disk," TR 002820, Dept. of Aerospace Engineering, Univ. of Michigan, 1971.